Construction and Building Materials xxx (2017) xxx–xxx

Contents lists available at ScienceDirect

Construction and Building Materials

journal homepage: www.elsevier.com/locate/conbuildmat

Combined NDT techniques in civil engineering applications: Laboratory and real test

Luigi Capozzoli, Enzo Rizzo *

CNR-IMAA, National Research Council – Institute of Methodology for Environmental Analysis, C.da S. Loja, 85050 Tito Scalo, Italy

HIGHLIGHTS

- NDT are able to investigate engineering structures.
- The best work for a geophysical approach is the multisensor use.
- The tests defined the NDT skill increasing the knowledge in the restoration phases.

ARTICLE INFO

Article history:
Received 21 November 2016
Received in revised form 6 July 2017
Accepted 18 July 2017
Available online xxxx

Keywords:
Non-destructive tests
Ground-penetrating radar
Electrical resistivity tomography
Infrared thermography
Geophysical laboratory test
In-situ applications

ABSTRACT

The damage of concrete structures calls for effective methods for condition evaluation and maintenance. The usual destructive testing has many disadvantages in Civil Engineering because involves the physical destruction of specimens to evaluate mechanical and structural characteristics. On the contrary, Non-Destructive Tests (NDT) are able to investigate different structures with high resolution, low time consuming and relative few costs. This resulted in development of several NDTs techniques for monitoring civil infrastructures. Accurate analysis of the physical parameters that characterize the structures is made possible by the spread of instruments that are actually more precise and economical. However, failure to use non-destructive tests effectively can be disastrous in operation of structures restoration or buildings rehabilitation. Applied geophysics is able to provide many information on the state of preservation and quality of engineering work. This work has investigated the skill of Ground Penetrating Radar (GPR) also applied in tandem with Infrared Thermography (IR) and Electrical Resistivity Tomographies (ERT) for the characterization and monitoring of building structures in laboratory and *in-situ* conditions. Two experimental cases are realized: in the first one GPR and ERT were performed in full scale laboratory conditions where a road segment was investigated in different conditions; in the second test, a radiant floor was investigated with comparison of results obtained with GPR and IR. The study demonstrates the feasibility of integrating the collected data obtained with non-destructive testing to enhance knowledge of engineering issues.

1. Introduction

The use of ground penetrating radar (GPR) in civil engineering provides many advantages, especially in the field of non-destructive tests where non-invasive, low costs and rapid monitoring techniques are strongly recommended. GPR is an active geophysical method based on transmissions of short electromagnetic (EM) energy pulses into the medium and analysis of scattering phenomenon due to variations of some physical properties as electrical conductivity, dielectric permittivity and magnetic permeability. GPR is currently used in civil engineering to solve different issues mainly related to the maintenance of the structures, evaluation of stability of concrete and masonry structures, structural health monitoring of infrastructure conservation, localization of buried services and pipes [1]. Great efforts are made to investigate GPR potentialities applied to testing asphalt pavements, to detect voids, fractures or other type of defects potentially dangerous for the conservation and utilization of roads [2,3], for pavement thickness measurements [4,5], to localize reinforcement in concrete pavement [6,7];to inspect industrial railway tracks and concrete bridges [8–11]; for moisture content analysis [12,13]. At the same time, GPR is widely used for localization of services and underground utilities in absence information [1,14,15], especially when excavation activities are necessary and it is impossible find projects and plans [16]. Moreover, the GPR should be used for

* Corresponding author.
E-mail address: enzo.rizzo@imaa.cnr.it (E. Rizzo).

http://dx.doi.org/10.1016/j.conbuildmat.2017.07.147
0950-0618/

restoration of important monuments [17–19]. GPR is often supported by other non invasive geophysical techniques in civil engineering applications, like acoustic techniques, infrared thermography (IRT) and electrical resistivity tomographies (ERT) [20].

ERTs are the less used method in the engineering field due to limitations in resolution, time consuming and surface sensor contact reliability. Anyway, they are well suited to evaluate variations of water content or presence of voids such as fractured and damage of concrete and masonry structures [21]. ERTs are an active geophysical method based on the investigation of horizontal and vertical electrical resistivity variations of the subsurface materials. However, the method is affected by limitations mainly due to the resolution and time to perform the investigations. A limitation for engineering application is the high electrical resistance between the electrode and the investigated media. In order to inject current on concrete structures, it is necessary to apply some shrewdness coming from the experience on the field. Anyway, ERT applications are well known to evaluate presence of defects in reinforced concrete structures [22–24], to monitor the temporal evolution of moisture distribution in concrete structures [25] and image masonry structures [26,27] but, actually, there are very few applications of this techniques in combination of GPR in the engineering field. The method is very able to identify moisture phenomena or presence of voids and fractures that could cause respectively a strong increase of conductivity and resistivity measured data supporting the GPR acquisitions that in humid or water saturated conditions suffers strong attenuation effects. Another advantage of resistivity methods is the low complexity of the processing phase respect to GPR elaboration. The present study has investigated the potentialities of this method to characterize and detect defects in engineering structures and support the interpretation of the GPR data in conductive conditions where attenuation of electro-magnetic (E-M) energy increases.

The last non-destructive testing (NDT) applied in this research was the Infrared Thermography (IRT) that represents a diagnostic remote sensing technique that consisting in measuring the energy that is naturally emitted from a body in the infrared field (between 1–20 μm) when its temperature is greater than zero degrees Kelvin, that is, the absolute temperature. Often GPR is used in tandem with IRT that represent another well-known non-destructive testing [20] based on use of an infrared camera able to measure and image the emitted infrared radiation from an object converting a thermal radiation pattern, into a visual image [28]. In the engineering field, the processing and interpretation of thermal images of building surfaces allows us to detect and survey hidden structures, zones affected by moisture and, patterns linked to the presence of decay pathologies such as deposits, biological patinas and cracks [29,30]. The IRT and GPR were integrated in order to improve confidence in defect detection and quantification or monitor bridge conditions [31–33]. The integrated use of the two techniques allows to reduce the limits of each techniques and to suggest using the capabilities characterizing each techniques, also in bridge deck condition testing. In particular IRT is less effective in terms of penetration depth while is characterized by a very high resolution; for this reasons can support effectively GPR to highlight critical zones occurring in the most superficial centimetres (up to a depth of 10 cm) [34]. The lower depth penetration of investigation characterizing the IR method is compensate by the high resolution of the method in surface investigation. In this work, we propose the use of IRT with GPR to reduce both the uncertainties of the geophysical method, mainly for the shallower layers, both increase the depth of investigation obtainable with the only use of IRT.

2. Aims and objectives

The paper highlights a particular attention on electromagnetic sensing technologies for their non-invasive characteristics to observe subsurface change of engineering infrastructures. In detail, in order to identify the capability of GPR to investigate civil engineering structures, a laboratory study case focused on use of GPR inspections, also in tandem with ERT, on asphalt and concrete pavement diagnostic is showed. A small road segment characterized by the presence of structural embedded defects and buried pipes was investigated with antennas with different operating frequencies. In this case, the experiment has evaluated the capability of each sensing technique to detect and characterize the different levels of the deformation size. Finally, the second application shows an integrated use of GPR and IRT to characterize a radiant floor heating system.

The paper is organized as follows. In the next section, the theoretical aspects are presented. The section 4 highlights the integration work with different NDT techniques in the laboratory (GPR and ERT) and in a gym (GPR and IRT). In the last two sections the results are discussed and a conclusion is defined.

3. Theoretical aspects

The electrical conductivity, dielectric permittivity and magnetic permeability regulate the velocity of propagation of EM waves and attenuation of EM energy. Analyses of variations of EM behaviour of the investigated medium provide good information about health and safety of civil structures. These variations generate reflections related to contrasts in EM impedance; further the electromagnetic characteristics of the subsoil influence hardly the velocity of propagation of electromagnetic waves and attenuation of the energy introduced in the subsoil. In low-loss conditions the velocity and the attenuation of e-m waves are [1,2]:

$$v = 1 \Big/ \sqrt{\varepsilon\mu} \tag{1}$$

$$\alpha = 0.5\sigma\sqrt{\mu/\varepsilon} \tag{2}$$

where ε is the dielectric permittivity, μ is the magnetic permeability and the σ is the electrical conductivity. At high frequencies, the electromagnetic fields propagate as waves through the medium and the previous equations become [3,4]:

$$v = 1 \Big/ \sqrt{\varepsilon\mu} = c \Big/ \sqrt{k} \tag{3}$$

$$\alpha = 0.5\sigma\sqrt{\mu/\varepsilon} = \sigma/2 \cdot \sqrt{k} \tag{4}$$

where $Z = \sqrt{\mu/\varepsilon} = Z_0/\sqrt{k}$ is the impedance of the investigated medium, Z_0 the impedance of free space and k the dielectric permittivity when the magnetic permeability considered negligible. The above two expressions show that the dielectric permittivity controls velocity while the electrical conductivity has a large effect on attenuation. These two parameters are the most important in GPR acquisitions that regulate the propagation phenomenon of e-m waves in the analysed medium and consequently the obtained results. A detailed description of the theory GPR is well described on [2,3] where are also discussed various applications of GPR in many field of research.

ERT is an electrical resistivity method based on the measurement of an electric field artificially created in the ground by suitable electronic devices, normally consist of two pairs of electrodes fixed in the ground, of which: a pair inject the current (I), the other the measuring circuit of the potential difference (dV) generated in the ground by the passage of the current itself.

Please cite this article in press as: L. Capozzoli, E. Rizzo, Combined NDT techniques in civil engineering applications: Laboratory and real test, Constr. Build. Mater. (2017), http://dx.doi.org/10.1016/j.conbuildmat.2017.07.147

The fundament of this technique is the Ohm's Law which indicates that the potential difference dV (V) at the ends of a conductor, at a given temperature T, is proportional to the electric current I (A) passing through it by means of a quantity constant and typical of the conductor, said resistance R (Ohm):

$$I = -dV/R \tag{5}$$

$$R = \rho L/A \tag{6}$$

where ρ (Ohm·m) is the electrical resistivity, L (m) is the conductor length, and A (m^2) is the conductor area. Generally, a switched square wave is the current waveform used. The data acquired are expressed in form of apparent resistivity. There are several configuration depending on the position of electrodes on the surface or borehole. The most used are generally, Wenner, Shlumberger, dipole-dipole and pole-pole arrays [35]. For the purpose of this work, we have used dipole-dipole and pole-pole configurations.

The dipole-dipole array is constituted by a current dipole and a potential dipole while in pole-pole array theoretically only one current electrode and one potential electrode are used (the other two are placed at distance which is more than 20 times the maximum separation between the first ones used in the survey). The apparent electrical resistivity values are then elaborated in terms of real ones and depth by means of inversion algorithm. The inversion procedure is usually to compute the 'best' set of resistivity values, which satisfies both the measured dataset and some a priori constraints, in order to stabilize the inversion and constrain the final image [35].

From theoretical point of view in the infrared method, the intensity and the spectrum of the energy naturally emitted from a body in the infrared field are functions only of the temperature of the body that emits this energy. This is the black body model that follows Stefan-Boltzmann's law, i.e.:

$$J = \sigma \cdot T^4 \tag{7}$$

where J is the exitance, that is the radiation emitted per unit of surface (W/m^2), σ is Stefan-Boltzmann's constant (5.67×10^{-8} $W/m^2 K^4$) and T is the absolute temperature (°K). The analysis of thermal variations by using heat diffusion laws allows us to identify surface characteristics of the materials as well as their physical condition [36]. It is also possible to identify spatial patterns that describe specific decay types either by examining each thermogram separately or by analysing the full multi-temporal IRT dataset using, for example, a data mining approach [37]. The acquisition of IR images could carried out in two ways: steady and transient. Steady thermograms give a static snapshot of the temperature measurement, while the transient methodology allows observation of a change in time of the surface temperature from a single thermogram. The heat source could be natural or artificial, in the case we define the thermography passive (more used for the historical buildings) and active, respectively. However, to better characterize the thermal behaviour of architectural surfaces characterized by a variegated material and decay pattern a significant contribution is provided by the analysis and processing of multitemporal thermal images [38].

4. Laboratory and field data: acquisition, processing and analysis

Two experimental activities were realized: EA1 and EA2.

The EA1 was conducted in a full scale laboratory and it was subdivided in two main phases:

- Phase A: in this phase, only GPR acquisitions were made on a road segment with a surface asphalt layer.
- Phase B: at this stage, GPR and ERT surveys were performed on a road segment after removal of asphalt layer.

The EA2 experiment was performed in a gym where GPR and IRT acquisitions were used in tandem.

4.1. EA1: laboratory case study

In the framework of the project, called Integrated System for Transport Infrastructures surveillance and Monitoring Electromagnetic Sensing (ISTIMES) funded research project [39], several experiments were realized at the Institute of methodologies for environmental analysis of the National Research Council (CNR - IMAA) in the Hydrogeosite laboratory located in Marsico Nuovo (PZ) [40]. The ISTIMES project was based on the implementation of a complex monitoring system based on satellite, aircraft and in-situ observation technologies able to detect displacements, dislocations and degradation phenomena, changes in physical and chemical conditions of engineering materials, congenital or induced structural defects of for transport infrastructures [37]. The laboratory is a large concrete pool of 252 m^3 ($12 \times 7 \times 3$ m) filled with silica sand (95% SiO_2, an average diameter of about 0.09 mm, porosity of about 45÷50% and hydraulic conductivity in the order of 10^{-5} m/s). The Hydrogeosite laboratory represents an intermediate stage between laboratory experiments and field survey. Therefore, it has the advantage to obtain controlled results, like in a laboratory experiment, but at scales comparable with the field ones [41]. In this context, a simulation of an engineering context was performed and, in a limited area of about 3×3 m, a road segment characterized by a multi-layer structure was built. In detail, the structure under test was made up of several layers, rebar and utilities (metallic and non-metallic pipes) for maximum a depth of about one meter (Fig. 1).

The asphalt layer was the shallow one with a thickness of about 0.05 m. The second layer (reinforced concrete slab) had a thickness of about 0.05–0.10 m and was reinforced with a 10×10 cm welded mesh (diameter of 0.06 mm). Two different layers of sand and conglomerate with varying thickness completed the road structure. The conglomerate level was thick approximately 0.20–0.25 m and supported the concrete slab. Beneath this layer there were two layers of sand, where in the first one three kind of pipes (steel, aluminium and plastic) were installed, while the second was characterized by a more compacted sand layer (Fig. 1). The materials have been chosen to cover as much as possible engineering applications. Generally, the pipes are realized in plastic and steel, but some structures like electrical conduits are realized in aluminium or fiberglass. The pipes were installed with the top at same depth of about 60cm and a reciprocal distance, calculated from the centre of each circumference, of 50 cm (steel and aluminium tubes) and 70 cm (plastic tubes). The tube diameters used ranged between 10 cm for the plastic tube (Pl in Fig. 1) and 6 and 4 cm for respectively aluminium (Al in Fig. 1) and iron pipes (St in Fig. 1). Finally, a groundwater was defined with a water level at 150–160 cm from the surface.

After the installation of the road structure, a simulated damage caused by a heavy track system was performed. The Fig. 2 highlights the dimension of the superficial deformation ranging between 1.50 and 3.00 mm (Fig. 2b). Finally, the subsidence zone was filled with a second shallow layer of asphalt (Fig. 2c). At this stage, the GPR measurements started with and without the asphalt layers, in order to have a comparison with the ERTs data.

The GPR investigations were made with a SIR-3000 GSSI Instrument coupled to 400, 900, 1500 and 2000 MHz antennas and metric encoder measuring wheel (Fig. 3). The data were gathered bidirectionally (see Fig. 4a) along parallel lines spaced 0.40 and 0.20 m respectively for the 400 and 900 antenna acquisitions.

Please cite this article in press as: L. Capozzoli, E. Rizzo, Combined NDT techniques in civil engineering applications: Laboratory and real test, Constr. Build. Mater. (2017), http://dx.doi.org/10.1016/j.conbuildmat.2017.07.147

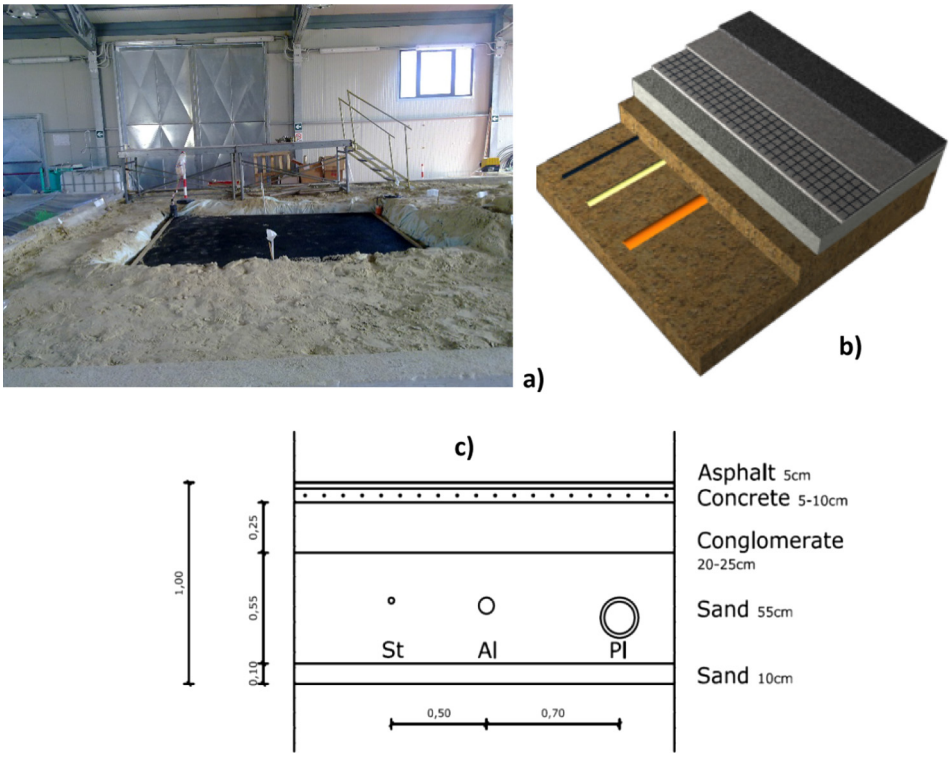

Fig. 1. Geometrical characteristics of the investigated test site. (a) A photo of the full scale laboratory where the road segment was installed; (b) 3D rendering of the test site plan; (c) the different layers with the thickness and the location of the different pipes (St: Steel; Al: aluminium; Pl: Plastic).

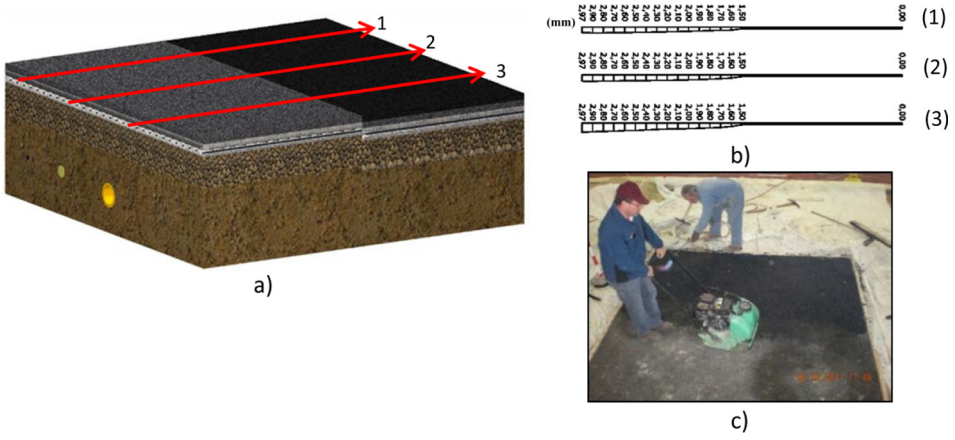

Fig. 2. Deformation phase. (a) longitudinal sections of the three topographic profiles; (b) topography profiles of the surface deformation expressed in mm; (c) re-asphalt of the subsidence zone.

The surveys realized at 1500 and 2000 MHz were realized with profiles placed every 0.10 m. We have used all these frequency that are generally used in engineering field test. In particular 400 MHz antenna are used to identify underground utilities while the other antenna are able to identify degradation phenomena occurring in the first centimetres of building works and are generally used in the restoration and rehabilitation fields thanks their higher resolution.

The investigations were made in two distinct phases characterized by the presence and absence of asphalt layer, in order to apply also the ERT methodology which needs both a physical contact between the sensors and the pavement both a low electrical resistance. For this reason, since the asphalt is composed by bitumen that is an excellent electrical insulator, it was necessary remove it before to start the resistivity acquisitions (see Fig. 4b).

The data had the same starting and finish point of acquisition and the processing strategy was completed, for each investigation phase, by a 3-D processing aimed to obtain a reconstruction of the objects present in the subsoil as rebar and pipes.

The raw-data have required a processing to improve the ratio signal noise and making easier the interpretation. Therefore, the data were processed using standard two-dimensional processing techniques by means of the software Reflex-W (Sandmeier scientific software). The whole process was schematized in Fig. 5. Processing steps can be summarized as follows:

- amplitude normalization to de-clip saturated traces by means of a polynomial interpolation procedure;
- dewow filter used to eliminate a possible low frequency part of the signal;

Please cite this article in press as: L. Capozzoli, E. Rizzo, Combined NDT techniques in civil engineering applications: Laboratory and real test, Constr. Build. Mater. (2017), http://dx.doi.org/10.1016/j.conbuildmat.2017.07.147

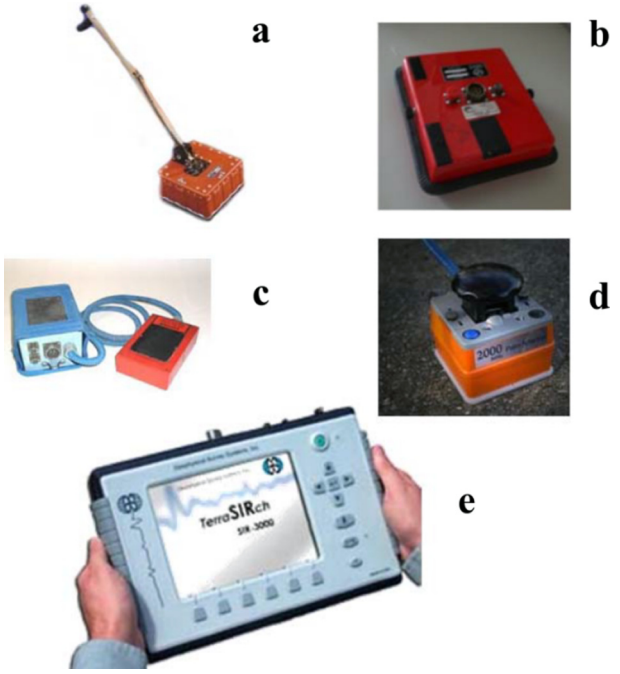

Fig. 3. GPR System Sir-3000 (e) coupled to four different antennas characterized by a central frequency of 400 (a), 900 (b), 1500 (c), 2000 (d) MHz.

- background removal to remove ringing effect. The filter is based of the calculation of an average of all background noise which has been subtracted from the data;
- energy gain based on a mean amplitude decay curve determined from all existing traces;
- declipping to reduce amplitudes values too high;
- againly a bandpass frequency filter was applied to reduce the increase of noise affecting the radargram caused by the gain function previously adopted;
- Kirchhoff 2D-velocity migration with a velocity estimated quantitatively estimating the diffraction hyperbolas generated by the objects placed in the subsoil.

After these steps (Fig. 5a), for the data acquired at the different frequencies 3D models were built interpolating data of the processed 2D-lines. A linear interpolation was made analyzing an area equal 1.5 times the minimum distance between the radargrams. Then the envelope of each trace of the 3D-files was calculated and showed in horizontal depth slices where the greater amplitudes were highlighted to identify engineering features (Fig. 5b).

The ERTs were acquired by a multichannel georesistivimeter (Syscal Pro by Iris Instrument) with a dipole-dipole and pole-pole arrays. The elaboration of the data was performed with the software Res3DInv [41] that provided to have vertical and horizontal resistivity slices of the investigated volume. In order to enhance the quality of contact between electrodes and surface, a high conductive medical gel was used between the circular steel electrodes and the pavement obtaining a contact resistances of about less than 1 KΩhm (Fig. 6).

The apparent resistivity acquired data are processed in order to characterize the 3D real electrical resistivity distribution removing spike values and electrical noise. The first step was to filter the data for the inversion, such as poor data detection. With Occam inversion based on a least-square method with the use of a smoothing operator and an additional contrast minimization the acquired data are inverted [42]. The smoothness method adjusts the two-dimensional resistivity model trying to iteratively reduce he difference between the calculated and measured apparent resistivity values expressed by the parameter called root mean-squared (RMS) error that provide a measurement of this difference expecting a better image from the combination of the two arrays. In the recorded cases, the RMS error was lower that 10%.

4.1.1. Phase A

The first stage was characterized by presence of the new asphalt layer after the damage simulation. GPR analysis with 400, 900 and 1500 MHz antennas was performed in order to characterize the road structure, fractures and deformations as well as buried pipes simulating presence of underground utilities. Moreover, the measurements were performed in a very humid background of the subsoil reproducing critical conditions for GPR due to the strong attenuation encountered by the EM waves in contexts both with a high water saturation degree and with clay and loamy sand that contributes to reduce the penetration depth of the e-m signal [43].

The GPR data with a 400 MHz antenna identified all the elements. In detail, the Fig. 7 shows a typical A-Scan (Fig. 7c) and the same 2D radargram, processed (Fig. 7d) and raw (Fig. 7e), acquired during the investigations. From previous unpublished GPR acquisition data in the full scale laboratory, we observe that a time windows of about 70 ns with a 400 MHz antenna should be a good value, in order to reach the bottom of the pool (around 3.00 m deep). The different layers of the panel are clearly visible for the presence of continuous parallel plane reflectors (coloured dash lines in Fig. 7c and d). The 2D acquisitions made possible the construction of 3D high reflection amplitude isovolumes that highlighted the presence of pipes (Fig. 7b). The presence of known reflectors provided to have good indicators to identify the velocity of propagation of the EM into the subsoil taking in account the effect of each layers. This information was used to perform a more

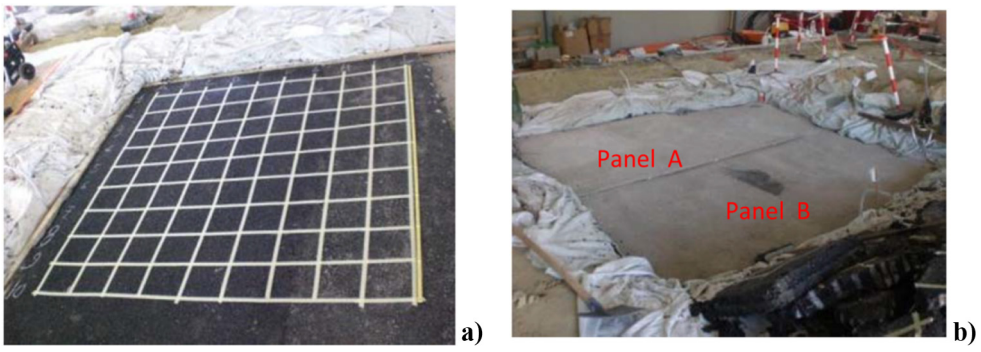

Fig. 4. View of the different phases of test study, (a) typical grid used to perform GPR acquisitions with 900 MHz antenna where profiles every 0.20 cm were acquired; (b) investigated panel after removing of asphalt layer.

Please cite this article in press as: L. Capozzoli, E. Rizzo, Combined NDT techniques in civil engineering applications: Laboratory and real test, Constr. Build. Mater. (2017), http://dx.doi.org/10.1016/j.conbuildmat.2017.07.147

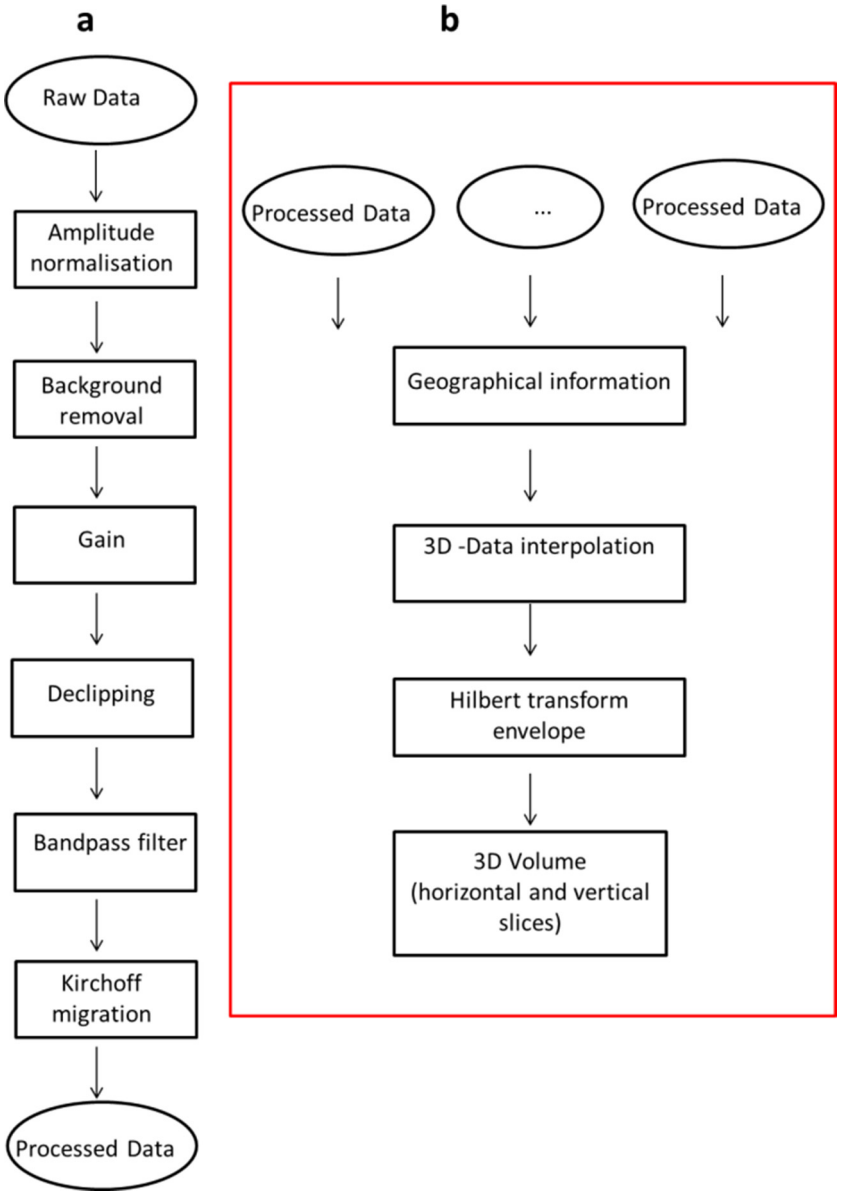

Fig. 5. Block diagram of the data processing for the GPR 2D (a) and 3D (b) acquisition.

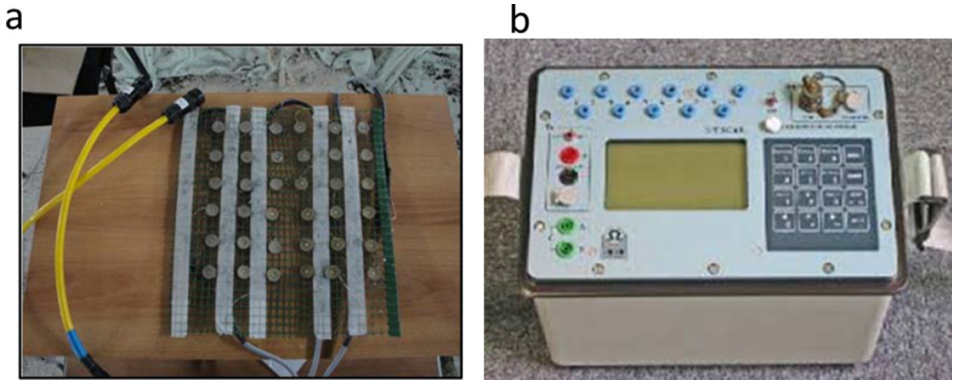

Fig. 6. Experimental equipment used for non-invasive geoelectrical measurements: (a) man-made sensors used to perform non-invasive ERTs realized with steel electrodes placed every 0.05 m in both the directions (n.36); (b) Georesistivemeter Syscal Pro (IRIS) with 96 channel.

Please cite this article in press as: L. Capozzoli, E. Rizzo, Combined NDT techniques in civil engineering applications: Laboratory and real test, Constr. Build. Mater. (2017), http://dx.doi.org/10.1016/j.conbuildmat.2017.07.147

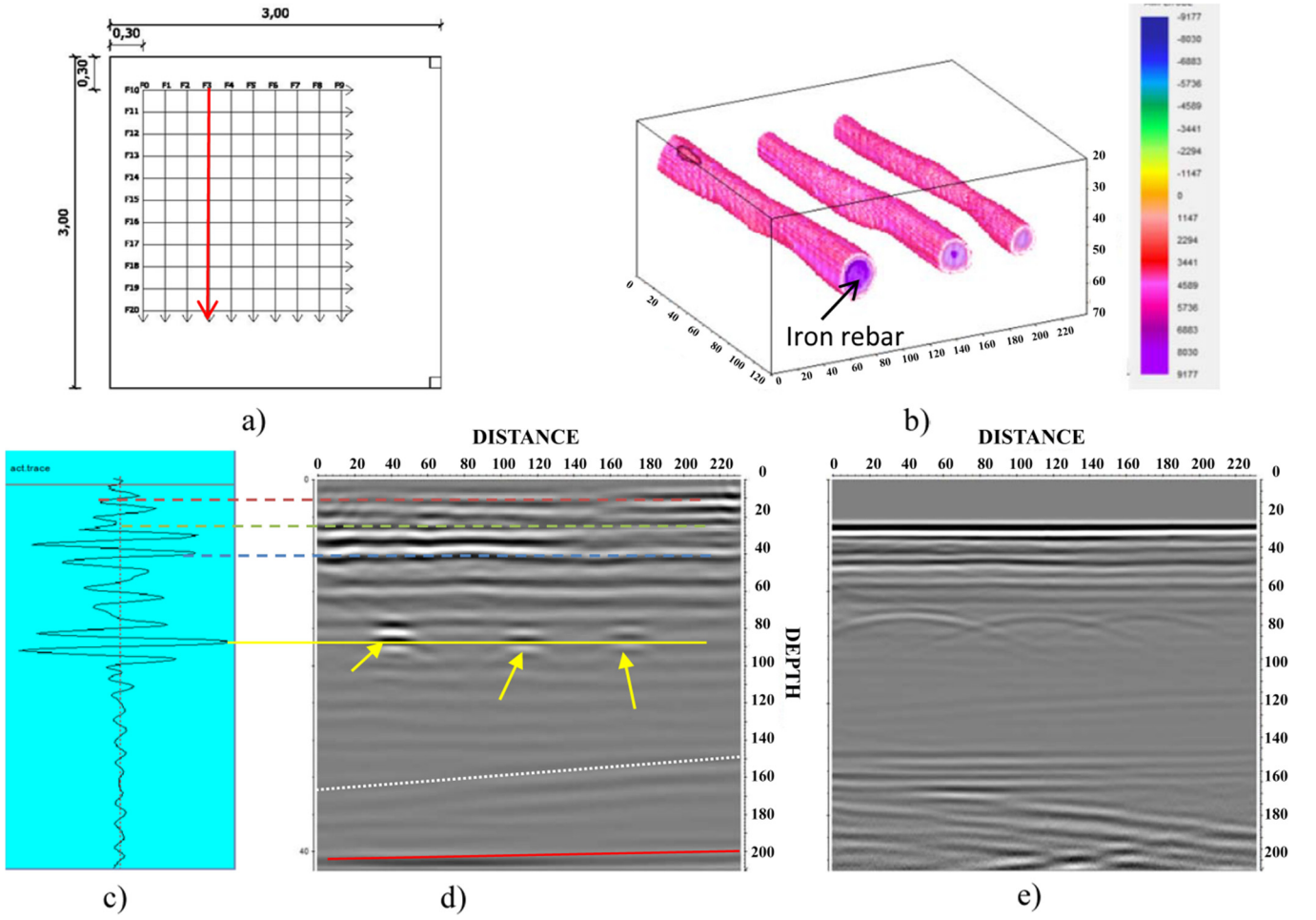

Fig. 7. Results obtained during the experimental first phase with 400 MHz antenna: grid of acquisitions with localization of showed investigated line (a), 3D *iso*-amplitude reflection volumes related to the presence of earthed pipes (b), processed A-scan (c), processed and raw B-scan in correspondence of F24 line (d and e).

effective migration of the data. Based on the GPR data interpretation and related equations, the dielectric values of the asphalt (∼6), concrete slab (∼10), conglomerate (∼13) and humid sand (∼25) layers were estimated. The estimated values are in the range that some authors found during other experiments [2–5,7,8,40]. Further, it is possible note how the presence of iron pipe generated a stronger reflection than other pipes; for this reason in 3D visualization, the greater isovolume is related to the iron pipe despite the other structures are characterized by greater diameters (Fig. 7b). Moreover, the water table and the concrete bottom of the pool are also detected as shown in Fig. 7d with white dashed line and red solid line.

The pipes are not well defined in the 900 and 1500 MHz radargrams. The time windows for the 900 and 1500 antennas were fixed to 15 ns, due to high water content conditions of the sand that has produced a strong attenuation of the EM signal. These acquisitions show a high resolution image of the surface concrete panel, highlighting useful information about defects and fractures. The radargrams plotted in Fig. 8 show the main fracture (red arrow) occurring at a distance of 120 cm from the acquisition starting point and the deformation of the layers interested by the breaking event (coloured dashed line). The hyperbolas related to the rebar of the welded wire mesh used to reinforce the concrete are also detectable. Two constructive layers charactering the panel are detectable: the asphalt layer and reinforced concrete slab delimitated by red and green dashed lines.

4.1.2. Phase B

The second stage started after removing of the asphalt layers. In this phase acquisitions with GPR coupled to 900, 1500 and 2000 MHz antennas were performed. In this case for the presence of the main visible central fracture, the investigation pavement area was divided in two zone (A and B) monitored separately by GPR (Fig. 9). The obtained results confirmed that the welded wire mesh, characterizing the concrete layer, suffers a considerable deformation perpendicularly to the breaking direction according the measurements realized in surface with a laser vertical meter. Moreover, the results allowed to identify the concrete and sand separation line and at a distance of about 1.00 m the presence of a plastic pipe (blue arrow) used in a subsequent experiment to simulate infiltration of water in the concrete slab, not detectable with the 900 MHz antenna. The deep pipes are not detected due to the high EM wave attenuation. Further, it is possible note a not homogenous thickness of the concrete layer that is more large in direction of the acquisitions.

We tried to perform 3D ERT acquisitions during the first stage, but the electrical contact between the sensors and the asphalt was very high. This effect prevented the injection of the current and defined the asphalt as a good electrical insulator. Therefore, after the asphalt layer removing action, several 3D ERTs were carried out in order to investigate the electrical resistivity distribution in the observed tests. In order to make geoelectrical measurements on concrete, a net of size of 0.25 × 0.25 m with 36 steel electrodes

Please cite this article in press as: L. Capozzoli, E. Rizzo, Combined NDT techniques in civil engineering applications: Laboratory and real test, Constr. Build. Mater. (2017), http://dx.doi.org/10.1016/j.conbuildmat.2017.07.147

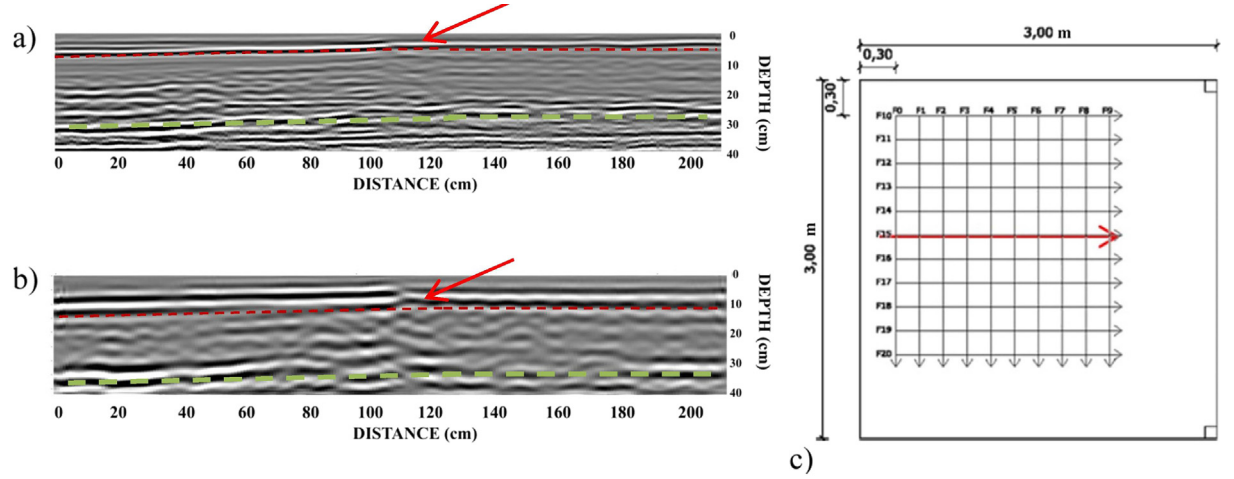

Fig. 8. The same transversal line investigated with 1500 (a) and 900 MHz (b) antennas with their localization during the first phase of the experiment (c).

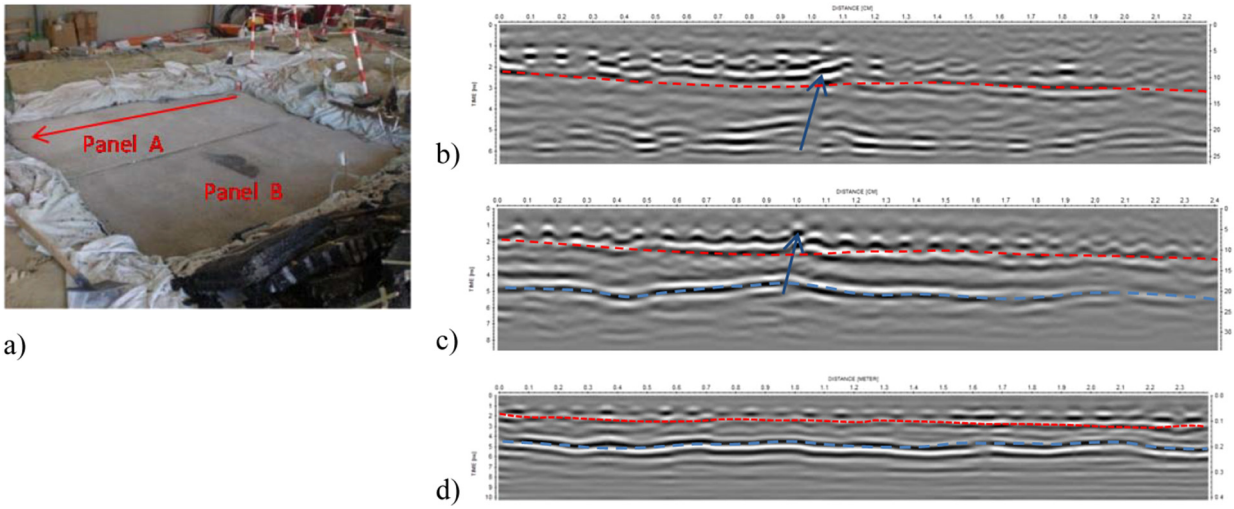

Fig. 9. F25 survey lines, 900 (b), 1500 (c), 2000 MHz (d) processed radargrams with respective localization (a) in the sub-panel A during the phase B.

were placed according a spacing of 0.05 m on six parallel distinct lines (Fig. 6a). This device was designed ad hoc, in order to make available several 3D ERTs where non-invasive and non-destructive tests are required. The 3D acquisitions were made only on part of the investigated panel (1 m^2) subdivided in sixteen squared net by dipole-dipole and pole-pole geoelectrical arrays (Fig. 9a). Then each acquired data set were merged together and a 3D inversion was performed by 3DResInv. The best results were obtained with pole-pole array with an investigation depth of about 0.24 m. The Fig. 10 shows five horizontal resistivity slices that describe the electrical behaviour of the investigated panel. At a depth of 0.04–0.08 m, a more resistive area near the left lower corner was due to the presence of a thickening of the concrete slab, that was realized non uniformly how yet showed with GPR. Moreover, the shallow resistivity maps highlight an inhomogeneous resistivity behaviour due to a different humidity of the concrete panel and at a different compaction of the concrete close the rebar. At a depth greater than 0.08 m, an increase of conductivity values demonstrate a change of the physical properties of the investigated volume in correspondence on the conglomerate layer composed by gravel and sand.

Finally more conductive areas are detectable at a depth greater than 0.17 m, in correspondence of the corners of the panel, due to different water content in the conglomerate layer placed at the bottom of the concrete slab. The Fig. 11 highlights the vertical sections of the 3D geoelectrical data. In detail, an electrical discontinuity related to transition from concrete layer to conglomerate layer was well delimited. It is clearly detectable the relative conductive behaviour of the deep conglomerate layer characterized by resistivity values lower than 50 Ωhm·m. Moreover, the shallow layer is characterized by relative high electrical resistive values (>150 Ohm*m) but with very high resistivity zones (>500 Ohm*m) and relative less high resistivity zones (between 150–400 Ohm*m). The electrical resistivity inhomogeneity of the shallow layer define or the location of different water content in the concrete panel or the location of some cracks not well visible in the GPR data due to presence of the rebars.

4.2. EA2: real case study

The second case study was investigated in a gym (Fig. 12) with GPR SIR-3000 (GSSI Instrument) coupled to 900 and 2000 MHz antennas and metric encoder measuring wheel) and IRT. IRT was performed with thermal imaging camera FLIR SC660 Series features detector FPA (Focal Plane Array) microbolometer. Such a

Please cite this article in press as: L. Capozzoli, E. Rizzo, Combined NDT techniques in civil engineering applications: Laboratory and real test, Constr. Build. Mater. (2017), http://dx.doi.org/10.1016/j.conbuildmat.2017.07.147

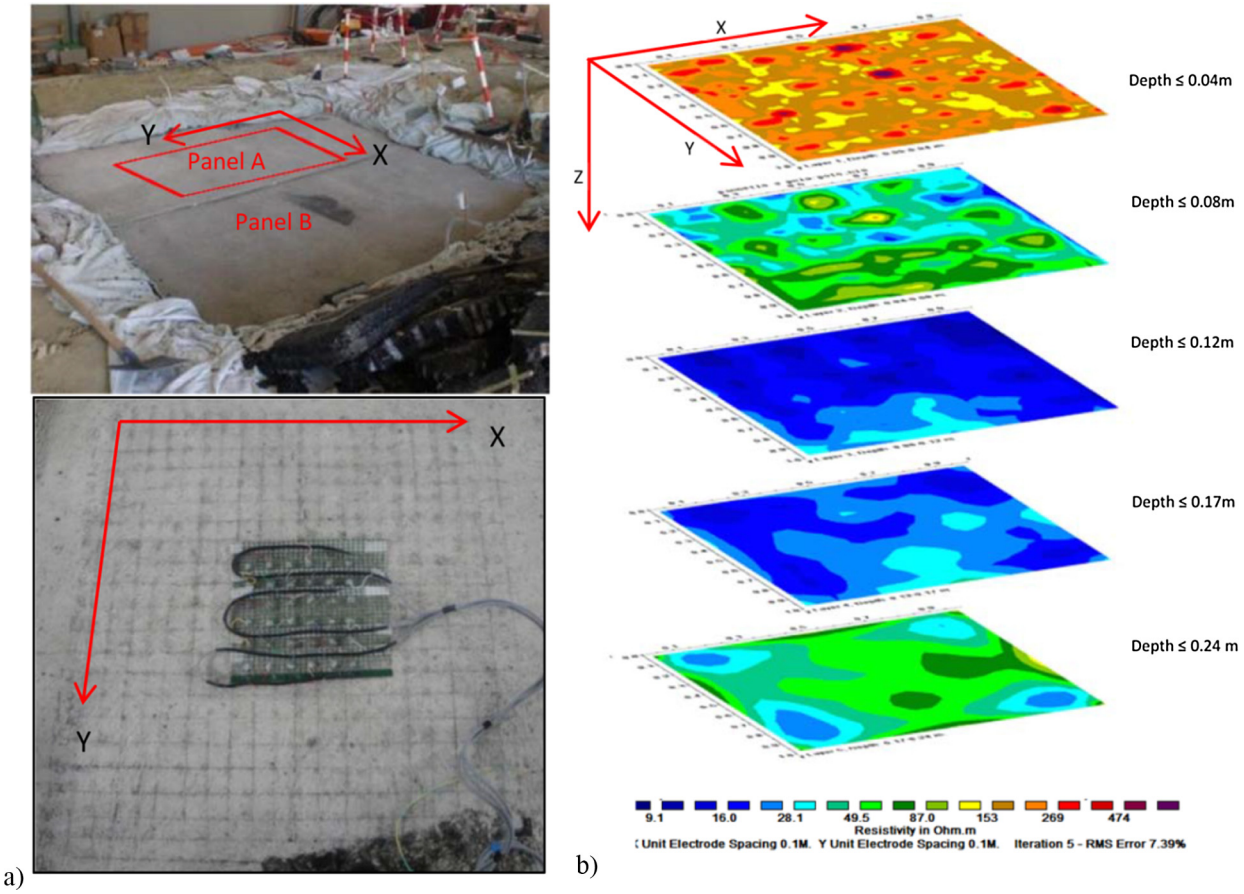

Fig. 10. (a) on the top the two panels and the location of the area where the 3D ERT acquisition were carried out; on the bottom a detailed grid of the 3D ERT acquisition; (b) Horizontal resistivity slices acquired by pole-pole geoelectrical array (maximum investigation depth 0.24 m).

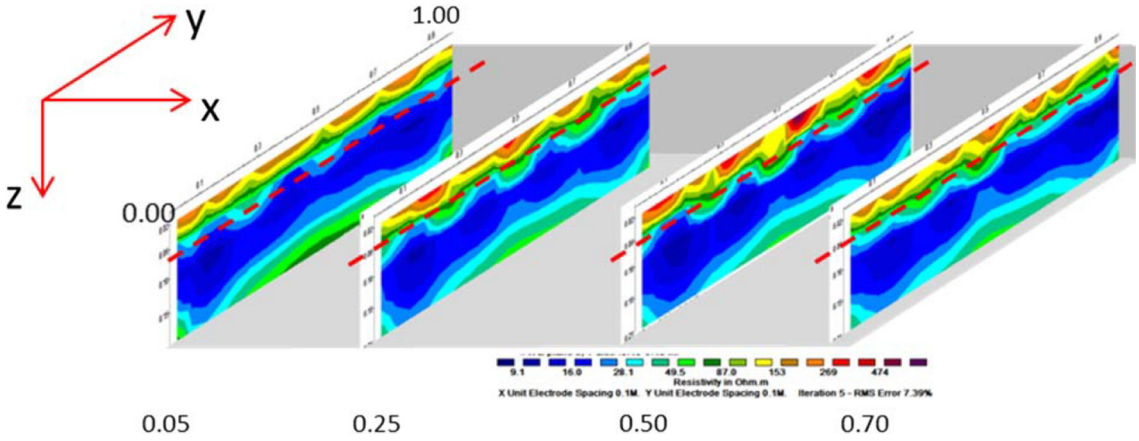

Fig. 11. Vertical resistivity slices acquired by pole-pole geoelectrical array. The dashed red lines is the limit between the concrete structure and the conglomerate layer. (For interpretation of the references to colour in this figure legend, the reader is referred to the web version of this article.)

thermovision system operates in the long-wave spectral range between 7.5–13.5 mm.

The target of the investigation was to characterize a radiant floor heating for the necessity to insert in the floor dowels to anchor steel plates of the volleyball net without breaking the tubes of the heating system. An approach based on the integrated use of GPR and IRT was adopted to identify the geometrical characteristics of the analysed structure since the project of the civil utilities was not available. In detail, two different portions of the floor were investigated in correspondence of the two posts site, where no dangerous or obstructing anchor system have to be installed on the ground. The two panels have a size of 1×1 m as showed in Fig. 13.

Multitemporal IRT datasets were acquired during cooling and heating transient conditions realized turning on and off the heating system. In this way, an enhancement of the knowledge was possible to investigate the thermal behaviour of the panels and define constructive characteristics. The interpretation of IRT images

Please cite this article in press as: L. Capozzoli, E. Rizzo, Combined NDT techniques in civil engineering applications: Laboratory and real test, Constr. Build. Mater. (2017), http://dx.doi.org/10.1016/j.conbuildmat.2017.07.147

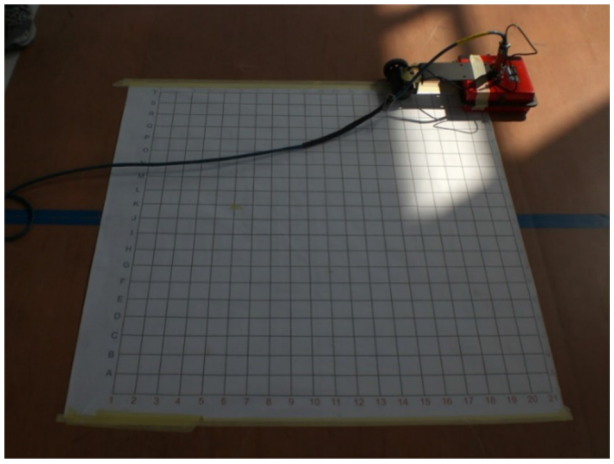

Fig. 12. One of the two investigated panels in a gym by 900 MHz antenna coupled to survey wheel and the acquisition stamp grid built ad hoc.

provided to map with accuracy the tubes spacing but the depth and the characteristics of the surrounding media was not well defined. On the contrary, GPR data were used to reconstruct the "stratigraphy" of the pavement that is composed by floor covering, insulation layer, damp proof membrane and hollow slab. A bidirectional survey grid was used to support acquisitions made with 900 and 2000 MHz antenna with a spacing lines respectively equal to 0.20 and 0.05 m. The 900 MHz results allowed us to describe the engineering structure composed by a floor system realized with precast concrete joists and hollow bricks. The 2 GHz results gave us information about the welded wire mesh used to reinforce the screed placed on the underfloor heating pipes.

5. Discussions

The two experimental activities described in the section 3 are all based on the use of GPR in tandem with other NDT. In particular, the first activity in the full-scale laboratory was realized by use of GPR and ERT in the second sub-phase. In the first phase, for explained limits due to the asphalt, was possible apply only GPR techniques. The obtained results showed the ability of GPR at a frequency of 400 MHz to identify and localize both metallic and non-metallic simulated underground utilities. Further, the stratigraphic boundaries due to the presence of a multilevel structure filling materials under the shallower layer realized in asphalt are detectable like showed in Fig. 6. Moreover, 400 MHz antenna did not allow to identify deformation phenomenon induced in the analysed segment cause its resolution. The surveys with 900 and 1500 MHz antenna have overcome some limitations thanks their better resolution but, obviously, the limited depth of investigation due to attenuation and scattering phenomena did not allow to identify the deeper pipes. Therefore, a "multifrequency" approach is highly desirable to effectively characterize engineering issues. At this stage, the 2000 MHz antenna did not work well, probably for scattering phenomenon induced by the type of asphalt realized with material with coarse grain. In the second stage, good results were achieved with all the frequencies used that, as showed in Fig. 8. In particular, it is notable like 2000 MHz and 1500 MHz antennas highlighted the deformation phenomenon and cracks characterizing the concrete slab.

Further, using equation 3 the dielectric permittivity of each layer was calculated and the obtained values were in good agreement with those indicated in [2–5,7,8,43], where for asphalt and concrete in wet conditions the relative dielectric constant ranges respectively between 6–12 and 10–20. Moreover, the indicated values are in good according to those identified by [4,44]. In particular for the asphalt, where has been found a dielectric permittivity value of 7. The higher value of dielectric permittivity was imputed to the presence of water in the loamy sand where the segment road was allocated that caused an increase of moisture in the upper layers.

The 3D ERT acquired on the concrete slab allowed us to identify more conductive zones correlated to the different water content, as the GPR data showed; on the contrary, the concrete structure characterized by rebar and inhomogeneity) was defined the electrical high resistive zones. The depth of investigation related mainly to the distance of the electrodes didn't provide to have some information about pipes but the results obtained with electrodes placed directly on concrete are encouraging like showed by RMS error that could be read like a quality control, always lower than 10%. In particular, the presence of the boundary between concrete and humid conglomerate was clear as showed in the horizontal and vertical slices showed in Figs. 11 and 12.

In EA2, GPR at the frequency of 900 and 2000 MHz identified the existing rebar (black circles in the layer delimited by a red dashed line in Fig. 14a) and the depth where fix the necessary studs. In particular, the technology used to build the precast

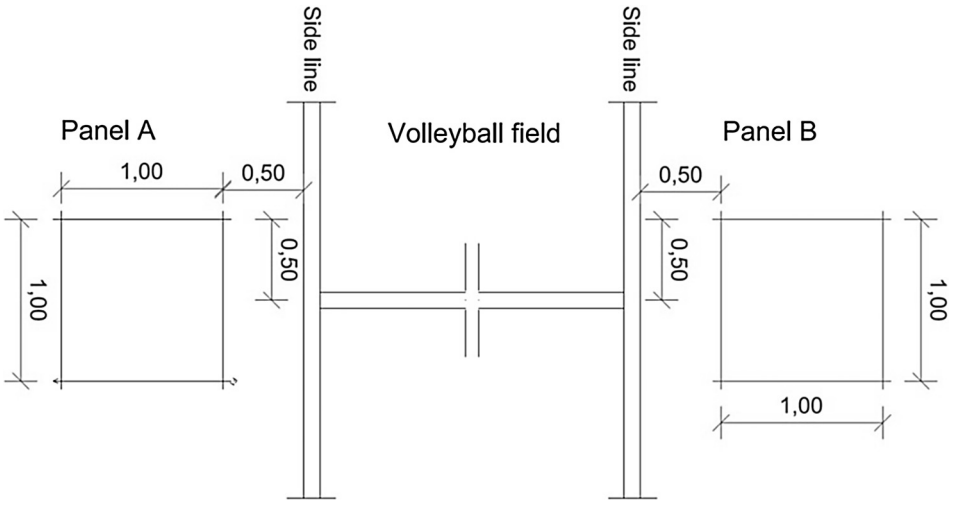

Fig. 13. Sketch of the investigated panels (Panel A and B).

Please cite this article in press as: L. Capozzoli, E. Rizzo, Combined NDT techniques in civil engineering applications: Laboratory and real test, Constr. Build. Mater. (2017), http://dx.doi.org/10.1016/j.conbuildmat.2017.07.147

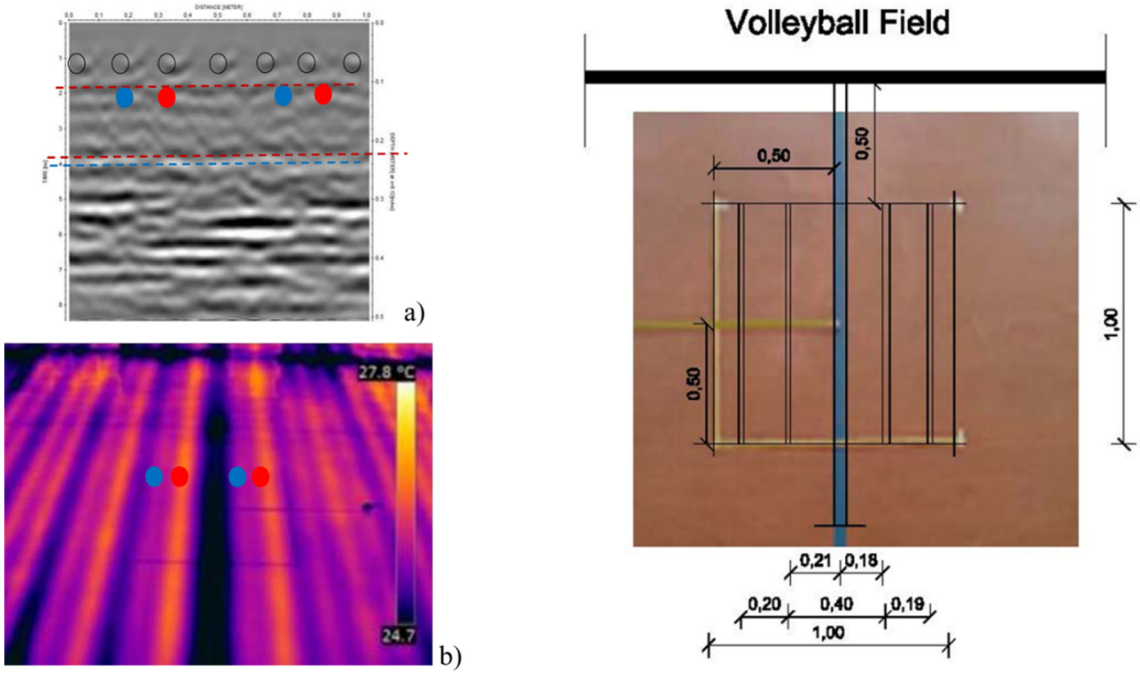

Fig. 14. (a) an example of GPR radargram acquired with 2 GHz antenna; (b) an example of IRT image. The blue and red circles indicate the cold and hot water pipes. (c) Interpreted reconstruction of plan distribution of pipes for panel B. (For interpretation of the references to colour in this figure legend, the reader is referred to the web version of this article.)

concrete floor was characterized at the frequency of 900 MHz while the pipes belonging to the radiant floor were detected with the 2000 MHz antenna. Moreover to confirm and validate the results obtained with GPR, for the analysed case, IR acquisitions gave us excellent results in according with radargrams. Therefore, only combined GPR and IRT results permitted to support the realization of the required anchor system, because it was possible to define the size of the plates and, in particular, the spacing of the holes housing the dowels of the volleyball posts. In other words, like for EX1, also in EA2 an integrated approach with multifrequency GPR information, subsequently validated with thermal images, was a good tool for non destructive testing to solve engineering questions.

6. Conclusions

The skill of GPR in the non-destructive testing field applied to civil engineering structures was evaluated with real and simulated tests in terms of depth of investigation and resolution. The test studies were realized with the presence of high water content, clay sand (as discussed in EA1) and multiple reflections imputable to different engineering structures (as demonstrated in EA2). In detail, a laboratory test has showed the importance of GPR to analyse critical problems related to maintenance and monitoring of civil engineering structures as fractures and deformation phenomena. The lab experiments highlighted the importance of the choice of the kind of antenna. The depth of penetration highlighted the crucial role of the antenna frequency to investigate subsoil at this frequency to localize underground utilities. Some problems are related to difficulties to identify small fractures or embed defect of the structure that encourage using higher frequencies characterized by higher vertical and lateral resolution. Therefore, the use of highest antenna frequency highlighted fractures and voids, but the high attenuation phenomena affected the em waves deep penetration. Moreover, the use of not-common NDT techniques, as the innovative 3D ERTs, permitted to obtain different information on the shallow concrete structure. Although, the electrical 3D maps were not able to detect the rebar geometries, as the GPR results highlighted, but highlight some information on the physical characteristic of the concrete panel. The results, despite the resolution and contact problems, show the usefulness and potentialities of the resistivity methods in the engineering field in particular to identify and monitor humid layers and compacted zone. Finally, the experiments have showed the skill of GPR in monitoring civil engineering applications where different 2D and 3D acquisitions have allowed information about positions and localizations of pipes and defects of the investigated medium. In particular, cracks and deformations were detected. For this reason GPR is a very important support among non-destructive tests thanks the high performance obtainable for detection and the ease of data interpretation. To have effective information it needs to have a good coverture of investigation and for this reason 3D acquisitions are strongly preferable. The real test has demonstrated that the comparison of results obtained via non-destructive tests are an optimal way to reduce uncertainties for engineering issues and increase the knowledge level in the decision phase on rehabilitation and restoration phases.

Acknowledgments

The authors thank the European Community's Seventh Framework Programme for the support on Hydrogeosite experimental activities (ISTIMES FP7 project). Moreover, they thank the Basilicata Volleyball Regional Federation and the Potenza Municipality for the permission to make the surveys in the gym. Finally, the authors thank the two anonymous reviewers and the guest editors for their fruitful suggestions and comments.

References

[1] E. Pettinelli, A. Di Matteo, E. Mattei, L. Crocco, F.O. Soldovieri, J. David Redman, A.P. Annan, GPR response from buried pipes: measurement on field site and

tomographic reconstructions, IEEE Trans. Geosci. Remote Sens. 47 (8) (Aug. 2009) 2639–2645.
[2] T. Saarenketo, NDT Transportation, in: H.M. Jol (Ed.), Ground Penetrating Radar: Theory and Applications, Elsevier, Amsterdam, 2009, pp. 395–444.
[3] D.J. Daniels (Ed.), Ground Penetrating Radar, 2nd Ed., The Institute of Electrical Engineers, London, United Kingdom, 2004.
[4] C. Plati, A. Loizos, Using ground-penetrating radar for assessing the structural needs of asphalt pavements, Nondestr. Testing Eval. 27 (3) (2012) 273–284.
[5] A. Loizos, C. Plati, Accuracy of ground penetrating radar horn-antenna technique for sensing pavement subsurface, IEEE Sensors J. 7 (5) (2007) 842–850.
[6] J. Stryk, R. Matula, Possibilities of ground penetrating radar usage within acceptance tests of rigid pavements, J. Appl. Geophys. 97 (2013) 11–26.
[7] S. Laurens, J.P. Balayssac, J. Rhazi, G. Klysz, G. Arliguie, Non-destructive evaluation of concrete moisture by GPR: experimental study and direct modeling, Mater. Struct. 38 (2005) 827–832.
[8] A. Benedetto, S. Pensa, Indirect diagnosis of pavement structural damages using surface GPR reflection techniques, J. Appl. Geophys. 62 (2007) 107–123.
[9] J. Hugenschmidt, R. Mastrangelo, GPR inspection of concrete bridges, Cem. Concr. Compos. 28 (4) (2006) 384–392.
[10] J. Hugenschmidt, C. Kasa, H. Kato, GPR for the inspection of industrial railway tracks, Near Surf. Geophys. 11 (5) (2013) 485–491.
[11] F. Tosti, A. Umiliaco, FDTD Simulation of the GPR signal for preventing the risk of accidents due to pavement damages, Int. J. Interdisciplinary Telecommun. Netw. (IJITN) 6 (1) (2014) 1–9.
[12] A. Benedetto, F. D'Amico, F. Fattorini, Measurement of moisture under road pavement: a new approach based on GPR signal processing in the frequency domain, International Workshop on Advanced Ground Penetrating Radar, Granada (ES), 2009.
[13] F. Tosti, E.C. Slob, Determination, by using GPR, of the volumetric water content in structures, substructures, foundations and soil, Civil Engineering Applications of Ground Penetrating Radar, Springer International Publishing, 2015, pp. 163-194.
[14] R.J. Yelf, Application of ground penetrating radar to civil and geotechnical engineering, Electromagn. Phenomena 7 (2007) 102–117.
[15] E. Van De Vijver, M. Van Meirvenne, T. Saey, S. Delefortrie, P. De Smedt, J. De Pue, P. Seuntjens, Combining multi-receiver electromagnetic induction and stepped frequency ground penetrating radar for industrial site investigation, Eur. J. Soil Sci. 66 (2015) 688–698, http://dx.doi.org/10.1111/ejss.12229.
[16] C. Plati, X. Dérobert, Inspection Procedures for Effective GPR Sensing and Mapping of Underground Utilities and Voids, with a Focus to Urban Areas, in: A. Benedetto, L. Pajewski (Eds.), Civil Engineering Applications of Ground Penetrating Radar, ISBN 978-3-319-04812-3, Springer, 2015.
[17] N. Masini, L. Nuzzo, E. Rizzo, Investigations for the study and the restoration of the Rose Window of Troia Cathedral (Southern Italy), Near Surface Geophys. 5 (2007) (2007) 287–300.
[18] N. Masini, R. Persico, E. Rizzo, Some examples of GPR prospecting for monitoring of the monumental heritage, J. Geophys. Eng. 7 (2010) 190, http://dx.doi.org/10.1088/1742-2132/7/2/S05.
[19] S. Piscitelli, E. Rizzo, F. Cristallo, V. Lapenna, L. Crocco, R. Persico, F. Soldovieri, GPR and microwave tomography for detecting shallow cavities in the historical area of "Sassi of Matera" (Southern Italy) Near Surface, Geophysics 5 (2007) (2007) 275–284.
[20] D.M. McCann, M.C. Forde, Review of NDT methods in the assessment of concrete and masonry structures, NDT&E Int. 34 (2) (2001) 71–84.
[21] A. Binley, A. Kemna, Electrical Methods, in: Rubin, Hubbard (Eds.), Hydrogeophysics, 2005, Springer, pp. 129-156.
[22] W. Daily, A. Ramirez, A. Binley, S. Henry-Poulter, Electrical Resistance Tomography of Concrete Structures, in: Proceedings of ECAPT94: 3rd European concerted action meeting on process tomography, Lisbon (Portugal) (Mar 24–27 1994).
[23] K. Karhunen, A. Seppanen, A. Lehikoinen, J. P. Kaipio, P.J.M. Monteiro, Locating reinforcing bars in concrete with electrical resistance tomography, Concrete Repair, Rehabilitation and Retrofitting II-Alexander et al. (Eds.), Taylor & Francis Group, 2009.
[24] K. Karhunen, A. Seppanen, A. Lehikoinen, P.J.M. Monteiro, J.P. Kaipio, Electrical resistance tomography imaging of concrete, Cem. Concr. Res. 40 (2010) 137–145.
[25] M. Buettner, A. Ramirez, W. Daily, Electrical resistance tomography for imaging the spatial distribution of moisture in pavement sections, Structural Materials Technology an NDT Conference, San Diego, CA (United States) (Feb 20–23 1996).
[26] R.C. Flint, P.D. Jackson, D.M. McCann, Geophysical imaging inside masonry structures, NDT E Int. 32 (8) (1999) 469–479.
[27] R. Keersmaekers, F. Van Rickstal, D. Van Gemert, Geo-electrical techniques as a non-destructive appliance for restoration purposes, Structural Analysis of Historical Constructions - Modena, Lourenço & Roca (Eds.), 2004.
[28] M.R. Clark, D.M. McCann, M.C. Forde, Application of infrared thermography to the non-destructive testing of concrete and masonry bridges, NDT E Int. 36 (2003) 265–275.
[29] E. Grinzato, P.G. Bison, S. Marinetti, Monitoring of ancient buildings by the thermal method, J. Cultural Heritage 3 (2002) 21–29.
[30] E. Rosina, E. Grinzato, Infrared and Thermal Testing for Conservation of Historic Buildings, Materials Evaluation, ASNT Journal, Aug 2001, Columbus (OH) USA, 2001.
[31] K.R. Maser, Integration of ground penetrating radar and infrared thermography for bridge deck condition testing, Mater. Eval. 66 (11) (2008).
[32] K.R. Maser, Integration of ground penetrating radar and infrared thermography for bridge deck condition evaluation, Non-Destructive Testing in Civil Engineering Conference, Nantes, France, June 30th–July 3rd, 2009.
[33] S. A. Dabous, S. Yaghi, S. Alkass, O. Moselhi, Concrete bridge deck condition assessment using IR Thermography and Ground Penetrating Radar technologies, Automation in Construction, in press.
[34] C. Maierhofer, R. Arndt, M. Röllig, R. Helmerich, A. Walther, B. Hillemeier, C. Rieck, Quantification of Voids and Delaminations in Real Concrete and Masonry Structures with Active Thermography: Case Studies, June 2006, doi: 10.13140/2.1.3437.2800, Conference: QIRT 2006, At Padova (Italy).
[35] M.H. Loke, R.D. Barker, Rapid least-squares inversion of apparent resistivity pseudosections by a quasi-Newton method, Geophys. Prospect. 44 (1996) 131–152.
[36] X.P.V. Maldague, Theory and practice of infrared technology for non-destructive testing, John Wiley & Sons, New York, USA, 2001.
[37] M. Danese, U. Demšar, N. Masini, M. Charlton, Investigating material decay of historic buildings using Visual Analytics with Multi-temporal Infrared Thermography data, Archaeometry 52 (3) (2010) 482–501, http://dx.doi.org/10.1111/j.1475-4754.2009.00485.x.
[38] M. Danese, L. Capozzoli, N. Masini, Research of the best spatial analysis method for IR multitemporal thermographic datasets. Cluster analysis to study cultural heritage Geophys. Res. Abstr. Vol. 12, 2010 EGU General Assembly 2010.
[39] M. Proto, M. Bavusi, R. Bernini, L. Bigagli, M. Bost, F. Bourquin, L.-M. Cottineau, V. Cuomo, P.D. Vecchia, M. Dolce, J. Dumoulin, L. Eppelbaum, G. Fornaro, M. Gustafsson, J. Hugenschimdt, P. Kaspersen, H. Kim, V. Lapenna, M. Leggio, A. Loperte, P. Mazzetti, C. Moroni, S. Nativi, S. Nordebo, F Pacini, A. Palombo, S. Pascucci, A. Perrone, S. Pignatti, F.C. Ponzo, E. Rizzo, F. Soldovieri, F. Taillade, Transport Infrastructure Surveillance and Monitoring by Electromagnetic Sensing: The ISTIMES Project. Sensors 2010, 10, 10620-10639.
[40] V. Cuomo, S. Fiore, V Lapenna, E. Rizzo, Hydrogeosite: nuovo laboratorio a grande scala per applicazioni geofisiche ambientali. Atti del "24° Convegno Nazionale del GNGTS" Roma 15 - 17 Novembre 2005, (2005).
[41] M.H. Loke, R.D. Barker, Practical techniques for 3D resistivity surveys and data inversion, Geophys. Prospect. 44 (1996) 499–523.
[42] S.C. Constable, R.L. Parker, C.G. Constable, Occams' inversion: A practical algorithm for generating smooth models from electromagnetic sounding data, Geophysics 52 (3) (March 1987) 289–300.
[43] F. Tosti, A. Benedetto, L. Bianchini Ciampoli, S. Lambot, C. Patriarca, E.C. Slob, GPR analysis of clayey soil behaviour in unsaturated conditions for pavement engineering and geoscience applications, Near Surface Geophys. 14 (2) (2016) 127–144.
[44] M.O. Gordon, K. Broughton, M.S.A. Hardy, The assessment of the value of GPR imaging of flexible pavements, NDT&E International, Elsevier Science, Vol. 31, No. 6, pp. 429–438, 1998.

Please cite this article in press as: L. Capozzoli, E. Rizzo, Combined NDT techniques in civil engineering applications: Laboratory and real test, Constr. Build. Mater. (2017), http://dx.doi.org/10.1016/j.conbuildmat.2017.07.147